IIETA International Information and Engineering Technology Association
Advancing the World of Information and Engineering

Journal Européen des Systèmes Automatisés
Vol. 59, No. 10, October, 2026, pp. 3021-3026
Journal homepage: http://iieta.org/journals/jesa

Assessment of a Stabilized Intermittency Transport Equation for Spalart-Allmaras Transition Modeling in Wind Turbine Airfoils

Valerio D'Alessandro*, Matteo Falone, Luca Giammichele, Renato Ricci

Dipartimento di Ingegneria Industriale e Scienze Matematiche, Università Politecnica delle Marche, Ancona 60131, Italy

Corresponding Author Email: v.dalessandro@univpm.it

Copyright: ©2026 The authors. This article is published by IIETA and is licensed under the CC BY 4.0 license (http://creativecommons.org/licenses/by/4.0/).

https://doi.org/10.18280/jesa.591021

Received: 1 August 2026
Revised: 13 October 2026
Accepted: 25 October 2026
Available online: 31 October 2026

Keywords:
transition models, Spalart-Allmaras model, wind turbine airfoils

ABSTRACT

This work aims to evaluate the effectiveness of recent progress of local correlation based laminar-to-turbulent transition modeling relying on the Spalart-Allmaras (SA) equation solution. These approaches are of particular relevance for the flow regimes encountered in wind energy applications where fully turbulent formulations are not always reliable for predicting aerodynamic force coefficients, a key aspect in the design of wind turbine blade sections. Building upon our previous implementation, we investigate the impact of strain-modulated and rotation-correction formulations in the SA turbulence model. Additionally, the intermittency equation is incorporated using a stabilized logarithmic formulation. A gradient-driven artificial viscosity is also employed in the intermittency equation to suppress unphysical Gibbs-like phenomena occurring in the transition region. The effectiveness and robustness of the aforementioned approaches are assessed by numerically reproducing flow fields around airfoils operating at Reynolds numbers typical of wind turbine blade sections. Results for the S809 airfoil are presented to demonstrate the model performance. The data indicate that the formulations here proposed are able to accurately capture the key aerodynamic phenomena governing this flow regime.

1. INTRODUCTION

The growing deployment of wind energy systems worldwide demands increasingly accurate and computationally efficient aerodynamic design tools. The aerodynamic performance of wind turbine blades depends critically on the behavior of the boundary layer over the blade sections, particularly on the laminar-to-turbulent transition process, which governs the distribution of skin friction and the onset of flow separation. At the Reynolds numbers typical of utility-scale rotors, significant portions of the blade surface may sustain laminar flow, making transition-sensitive modelling a key ingredient for reliable force-coefficient predictions.

Reynolds-Averaged Navier-Stokes (RANS) approaches represent the only feasible strategy for industrial aerodynamic workflows. However, fully turbulent RANS closures are inadequate in transitional regimes, as they tend to overpredict skin-friction drag and misplace separation onset errors that propagate directly into blade-element momentum calculations and energy yield estimates. To address this limitation, several local correlation-based transition models (LCTMs) have been integrated into the RANS framework. Among the most widely adopted formulations is the $\gamma - \widetilde{Re}_{\theta,t}$ model of Menter et al. [1, 2]. More recently, the coupling of intermittency-based transition models with the Spalart-Allmaras (SA) one-equation turbulence model [3] has attracted growing attention, owing to the reduced number of partial differential equations to be solved and the well-established robustness of the SA framework [4, 5].

Despite the progress made, critical numerical challenges remain largely unaddressed in the literature. In particular, the intermittency transport equation is inherently prone to instabilities: negative intermittency values cause divergence, while unphysical overshoots beyond the physical range can trigger floating-point exceptions. A logarithmic reformulation of the intermittency, which inherently enforces positivity, was preliminarily explored by the authors [5, 6]. In addition, Gibbs-like pressure oscillations near the transition front represent a further unresolved numerical artefact that compromises the accuracy of surface pressure predictions, particularly at moderate-to-high angles of attack.

The present paper addresses these open issues and contributes to the development of robust and accurate models for investigating the aerodynamic performance of airfoil profiles in wind energy applications. Building upon our previous implementations [5, 6], the transport equation for the intermittency is rewritten in logarithmic form. Moreover, a stabilization strategy was introduced by means of limiting procedure based on the artificial energy associated to γ that bounds excessively positive values. A gradient-driven artificial viscosity term is also introduced to suppress spurious pressure oscillations in the transition region. These stabilization strategies are combined with two formulations of the SA production term: the rotation-corrected variant and the strain-modulated production approach. Finally, the robustness and the reliability of the proposed models are benchmarked against flow fields around the S809 airfoil operating over a

range of Reynolds numbers typical of wind turbine blade sections.

The paper is organized as follows: in Section 2 the governing equations and the proposed modelling strategy are presented; Section 3 describes the numerical approximation, while Section 4 discusses the results for benchmark airfoils. Finally, Section 5 draws the main conclusions.

2. GOVERNING EQUATIONS

In this section, the governing equations adopted in this work are introduced. All the flow models are based on the incompressible RANS framework in which continuity and momentum conservation are defined as follows:

$$\frac{\partial u_j}{\partial x_j} = 0 \tag{1}$$

$$\frac{\partial u_i}{\partial t} + \frac{\partial}{\partial x_j}(u_i u_j) = -\frac{\partial p}{\partial x_i} + \frac{\partial}{\partial x_j}\left[2(\nu + \nu_t)S_{ij}\right] \tag{2}$$

In the above equations, u_i is the *i*-th component of the velocity vector, $p = P/\rho$ denotes the pressure divided by the density, S_{ij} is the strain rate tensor, and ν represents the kinematic viscosity.

2.1 Turbulence model

Turbulence effects are taken into account by adopting the SAs model:

$$\frac{\partial \tilde{\nu}}{\partial t} + u_j \frac{\partial \tilde{\nu}}{\partial x_j} = P_{\tilde{\nu}} - D_{\tilde{\nu}} + \frac{c_{b2}}{\sigma}\frac{\partial \tilde{\nu}}{\partial x_j}\frac{\partial \tilde{\nu}}{\partial x_j} + \frac{\partial}{\partial x_j}\left[\left(\nu + \frac{\tilde{\nu}}{\sigma}\right)\frac{\partial \tilde{\nu}}{\partial x_j}\right] \tag{3}$$

In which the production term, $P_{\tilde{\nu}}$, and destruction one $D_{\tilde{\nu}}$ are evaluated as:

$$P_{\tilde{\nu}} = c_{b1}\tilde{S}\tilde{\nu}$$
$$D_{\tilde{\nu}} = c_{w1} f_{w1} \frac{\tilde{\nu}^2}{d^2} \tag{4}$$

Conversely, the turbulent viscosity, ν_t, is evaluated starting from on $\tilde{\nu}$:

$$\nu_t = f_{v1}\tilde{\nu} \tag{5}$$

The closure functions for Eqs. (3) and (4) are the same adopted in the study [7]. Specifically, for $\tilde{S}$ in the production term, two different formulations were adopted. The first one, denoted as SA-R1 in this work, is derived from Dacles-Mariani et al. [8]. It aims to empirically calibrate the production term for vortex-dominated flow reducing the eddy-viscosity in the regions where the vorticity overcomes the strain rate introducing a rotation correction as follows:

$$\tilde{S} = [\Omega + min(0, S - \Omega)] + \frac{\tilde{\nu}}{k^2 d^2} f_{v2} \tag{6}$$

The second correlation for $\tilde{S}$, here called SA-SMP, is a strain-modulated production approach that follows the rationale of Baldwin and Barth [9]:

$$\tilde{S} = S\left(\frac{1}{\chi} + f_{v1}\right) \tag{7}$$

2.2 Local correlation-based transition model

Laminar-to-turbulent transition is considered by introducing the transport equations for both the intermittency, γ, and transition onset momentum thickness Reynolds number, $\widetilde{Re}_{\theta,t}$, here not reported for sake of compactness. For further detail, please refer to the study [7].

In this context is important remark that intermittency transport equation is reformulated, in logarithmic form, where $\tilde{\gamma} = \log(\gamma)$. This strategy inherently ensures the positivity of the variable. Additionally, its smoother distribution enhances numerical robustness and stability. The resulting transport equation for $\tilde{\gamma}$ reads:

$$\frac{\partial \tilde{\gamma}}{\partial t} + u_j \frac{\partial \tilde{\gamma}}{\partial x_j} = P_{\tilde{\gamma}} - D_{\tilde{\gamma}} + \frac{\partial}{\partial x_j}\left[(\nu + \nu_t)\frac{\partial \tilde{\gamma}}{\partial x_j}\right] + (\nu + \nu_t)\frac{\partial \tilde{\gamma}}{\partial x_j}\frac{\partial \tilde{\gamma}}{\partial x_j} \tag{8}$$

2.3 Stabilization of the intermittency

The logarithmic formulation for intermittency ensures a lower bound to the variable that cannot be negative. However, this treatment lacks any mechanism to prevent excessively high positive values of $\tilde{\gamma}$, which can trigger the blow up of the computation. In this context, we have developed a method to bound $\tilde{\gamma}$, inspired by the strategy proposed by Allmaras and Johnson [10]. Specifically, Eq. (8) is multiplied by the intermittency itself, resulting in:

$$\frac{\partial \tilde{e}}{\partial t} + u_j \frac{\partial \tilde{e}}{\partial x_j} = \tilde{\gamma}(P_{\tilde{\gamma}} - D_{\tilde{\gamma}}) + \frac{\partial}{\partial x_j}\left[(\nu + \nu_t)\frac{\partial \tilde{e}}{\partial x_j}\right] + (\tilde{\gamma} - 1)(\nu + \nu_t)\frac{\partial \tilde{\gamma}}{\partial x_j}\frac{\partial \tilde{\gamma}}{\partial x_j} \tag{9}$$

where, $\tilde{e} = \tilde{\gamma}^2/2$ is the artificial energy associated with $\tilde{\gamma}$.

The integration of Eq. (9) over a domain in which $\tilde{\gamma}$ is positive and its value is equal to 0 on the boundary, leads to the following conditions to guarantees that the artificial energy decrease in time, preventing high positive values of the intermittency [7]:

$$\tilde{\gamma}(P_{\tilde{\gamma}} - D_{\tilde{\gamma}}) < 0$$
$$(\tilde{\gamma} - 1)(\nu + \nu_t)\frac{\partial \tilde{\gamma}}{\partial x_j}\frac{\partial \tilde{\gamma}}{\partial x_j} < 0 \tag{10}$$

The first condition is always satisfied because $\tilde{\gamma}$ is greater than 0 thanks to its formulation and the production term is smaller than the destruction one. On the other hand, the second constrain in Eq. (10) leads to:

$$\tilde{\gamma} < 1 \tag{11}$$

This latter is guaranteed through a clipping procedure applied at the end of the solution algorithm.

In our computations, we noticed that the stabilization strategies described above are not sufficient to obtain a smooth reconstruction of the flow field. Indeed, in several cases a Gibbs-like oscillations were observed in the pressure distribution around the air foil surface, in correspondence of the transition region. To suppress spurious pressure fluctuations, we have introduced a gradient-driven artificial

viscosity term in $\tilde{\gamma}$ equation, as follows:

$$\frac{\partial \tilde{\gamma}}{\partial t} + u_j \frac{\partial \tilde{\gamma}}{\partial x_j} = P_{\tilde{\gamma}} - D_{\tilde{\gamma}} + \frac{\partial}{\partial x_j}\left[(\nu + \nu_t + \nu_{art})\frac{\partial \tilde{\gamma}}{\partial x_j}\right] + (\nu + \nu_t)\frac{\partial \tilde{\gamma}}{\partial x_j}\frac{\partial \tilde{\gamma}}{\partial x_j} \quad (12)$$

in which

$$\nu_{art} = c_{art}\,\Delta\,|\nabla \tilde{\gamma}| \quad (13)$$

Being c_{art} the artificial viscosity scaling coefficient and Δ the characteristic dimension of the grid's cell. In this work, the latter is considered as the cube-root of the cell's volume.

3. NUMERICAL APPROXIMATION

The governing equations above introduced are discretized in space using the unstructured, collocated finite volume framework provided by the foam-extend v5.0 library, a fork of the widely used OpenFOAM code. The numerical solutions are achieved using SimpleFoam, the steady-state solver for incompressible flows available in foam-extend that adopts the SIMPLE algorithm for pressure-velocity coupling.

In all simulations presented in this study, diffusive terms and pressure gradients are approximated using second-order accurate central schemes. On the other hand, convective terms are approximated using a second-order accurate linear-upwind scheme. The resulting linear systems for the momentum, $\tilde{\nu}$, $\tilde{\gamma}$, and $\widetilde{Re}_{\theta,t}$ equations are solved using a preconditioned bi-conjugate gradient method with a DILU preconditioner. By contrast, the pressure equation is solved using a preconditioned conjugate gradient solver combined with a diagonal incomplete Cholesky preconditioner.

A local convergence tolerance of 10^{-6} is prescribed for the pressure equation, whereas the other linear systems are considered converged once the residuals reach machine precision.

All simulations are performed on a distributed-memory parallel Debian Linux cluster composed of four Intel Xeon 6238R nodes, providing a total of 192 CPU cores operating at 2.2 GHz. Each computation typically employs 24 CPU cores. The foam-extend library is build using the GCC 10.2.1 compiler, and parallel execution is managed through the MPICH 3.3.1 MPI implementation, also built with GNU compilers.

4. RESULTS

In this section, we assess the predictive performance of the transition modeling approaches proposed in this work. The airfoils S809 operating at Reynolds numbers of $1{\cdot}10^6$ and $2{\cdot}10^6$ is selected as benchmark. This airfoil, depicted in Figure 1, is widely used in wind turbine applications and is well documented in literature [11], providing reliable reference data for the considered flow conditions while retaining a sufficient level of flow complexity, that includes the manifestation of a laminar separation bubble on both suction and pressure sides, followed by a laminar-to-turbulent transition. For these reasons, it represents suitable test cases for evaluating the developed approach over a range of Reynolds numbers typical of airfoil adopted in wind turbine applications.

The main aerodynamic parameters will be considered to quantitatively evaluate the effectiveness of the numerical results:

i. lift coefficient - C_l
ii. drag coefficient - C_d
iii. pressure coefficient - C_p

The computations were performed employing a structured O-type grid characterized by a number of cells of about $5{\cdot}10^5$ and an inflow and outflow boundaries distance of about 100 chord lengths away from the airfoil to avoid any influence of the boundary conditions on the results. The grid cells were clustered on the airfoil surface, adopting a height of the first cell set to guarantee $O(y^+) \leq 1$.

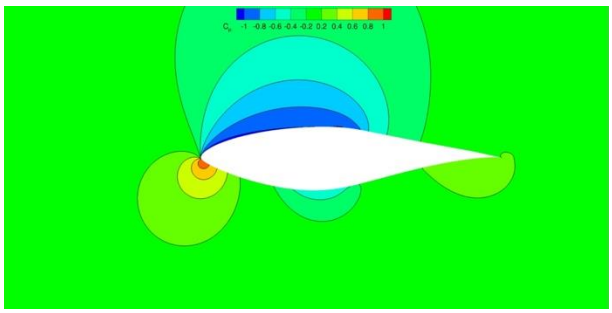


Figure 1. S809, Re = $2{\cdot}10^6$, α = 4°, pressure coefficient contour plot

Figures 2 and 3 show the pressure coefficient distribution around the airfoil surface at an angle of attack of 4° and 8° respectively and for a Reynolds number of $2{\cdot}10^6$. It is evident that the developed models are able to capture the flow features for the considered configurations.

In particular, Figure 2 provides evidence that both SA-R1 and SA-SMP formulations reproduce the flat plate-like behavior of the first half of the suction side highlighted in the experimental tests. More in depth, it is important to remark that the adoption of the rotation correction is effective in correctly reproduce the laminar separation bubble on the upper surface as well as on the lower one, as noticeable by the "knees" on the C_p distribution. Conversely, the SA-SMP model shows little discrepancies with respect to the experimental data.

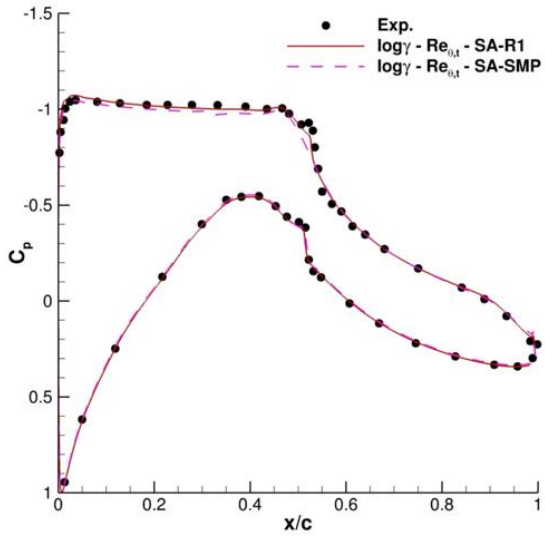


Figure 2. S809, Re = $2{\cdot}10^6$, α = 4°, pressure coefficient distribution

On the other hand, the results obtained for α = 8° are basically the same for the two approaches here investigated and, more important, they are in an excellent agreement with the experimental data provided by Somers. Also in this case our approaches are accurate in predict the laminar separation bubble followed by laminar-to-turbulent transition.

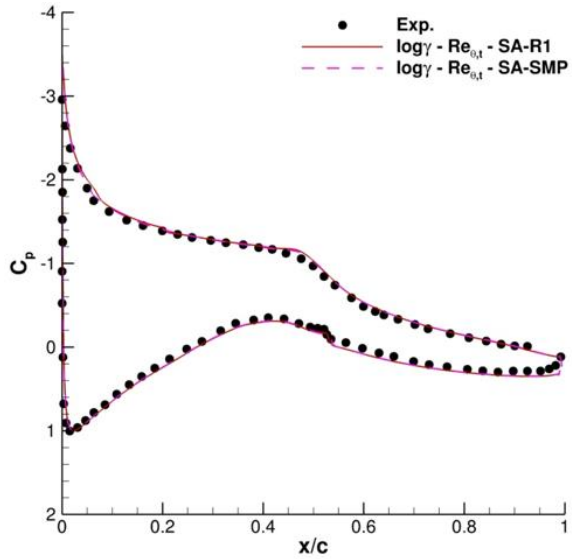


Figure 3. S809, Re = 2·10^6, α = 8°, pressure coefficient distribution

By contrast, when angles of attack within the stall regime are considered, the results highlight the limitations of the models adopted in this study. This behavior is clearly illustrated by the pressure coefficient distributions along the surfaces of the S809 airfoil at α = 12°, depicted in Figure 4. For this specific flow condition, the SA-R1 and SA-SMP formulations exhibit non-negligible discrepancies. In particular, the SA-R1 approach allows for a proper reconstruction of the C_p distribution on the pressure side and shows a slight underestimation of the pressure recovery downstream of the suction peak on the suction side. By contrast, the results obtained with the SA-SMP model deviate significantly from the experimental data.

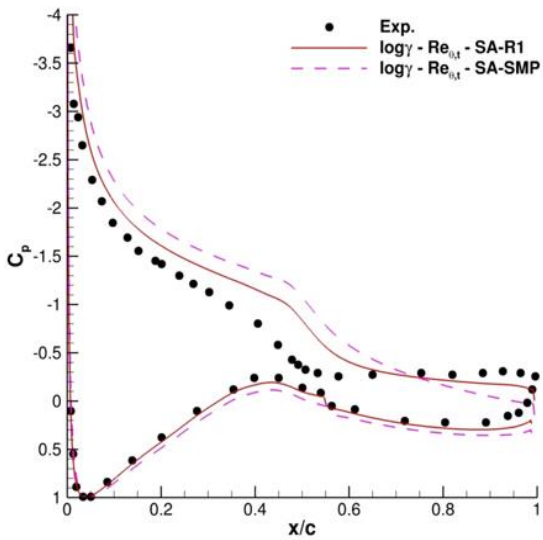


Figure 4. S809, Re = 2·10^6, α = 12°, pressure coefficient distribution

The ability of the proposed models to accurately predict the aerodynamic performance of the considered airfoil, at least up to stall onset, is further corroborated by the lift and drag coefficient trends shown in Figures 5 and 6. Specifically, these results confirm the findings reported in our previous work [7]: the developed models demonstrate effectiveness, efficiency, and robustness in predicting C_l and C_d at angles of attack preceding the stall region. Beyond stall onset, a tendency to overestimate the aerodynamic coefficients becomes apparent, likely due to the limited capability of the proposed formulations to resolve strongly separated flows, as is typical of RANS-based approaches. Nevertheless, the model incorporating rotation correction (SA-R1) is able to qualitatively capture the stall behavior.

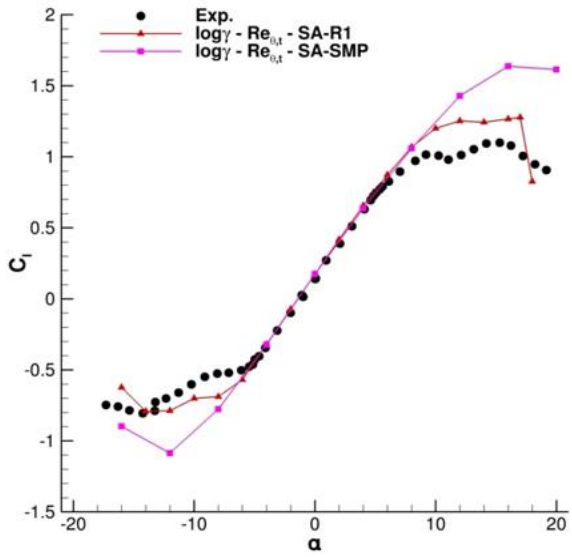


Figure 5. S809, Re = 2·10^6, lift coefficient

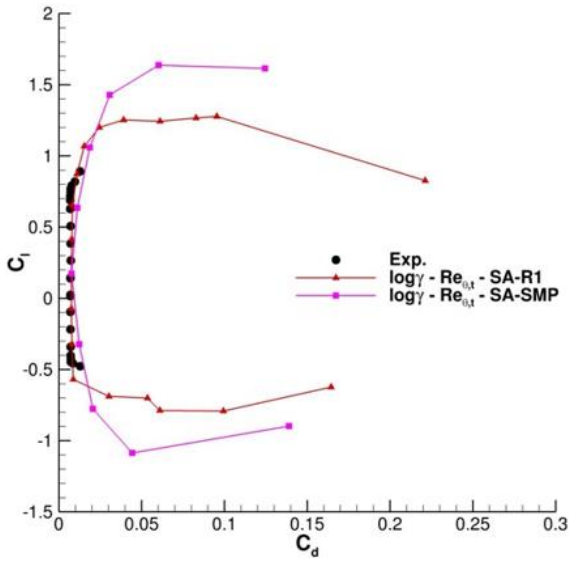


Figure 6. S809, Re = 2·10^6, eiffel polar

A second campaign of computations was conducted for the S809 airfoil operating at a Reynolds number Re = 1·10^6. In these simulations, in contrast to the case at Re = 2·10^6, local fluctuations of the pressure coefficient are observed in the vicinity of the laminar-to-turbulent transition region. The phenomenon confirms the findings of our previous work [7], where it was shown that, in case of airfoil for wind turbine

applications, the less is the operative Reynolds number, the more is the possibility to experience Gibb-like oscillations.

In particular, this occurs at high angles of attack, where the lift coefficient departs from its linear trend. Figure 7 and Figure 8 illustrate this behavior for the configuration Re = $1 \cdot 10^6$ and α = 8°. It is worth noting that adopting $c_{art} \geq 10^{-5}$ effectively damps the numerical oscillations on the suction side of the airfoil (see Figure 7), whereas smaller values are insufficient for this purpose.

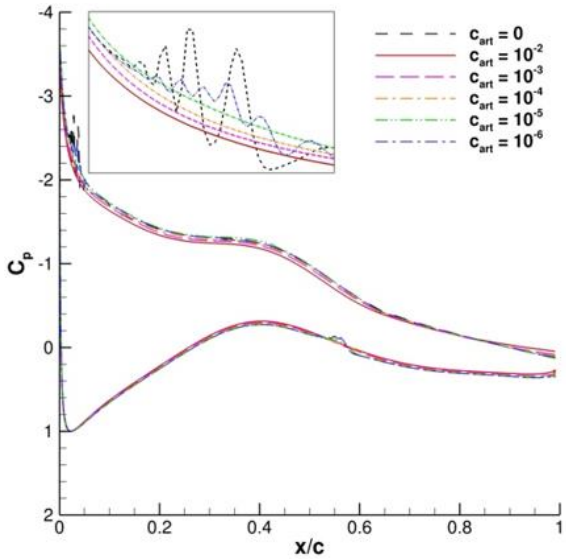


Figure 7. S809, Re = $1 \cdot 10^6$, α = 8°, effect of artificial viscosity - suction side

By contrast, an appropriate choice of the artificial viscosity scaling coefficient is critical to obtain a physically consistent solution on the pressure side. In fact, as can be seen in Figure 8, an excessive amount of artificial viscosity (i.e. $c_{art} \geq 10^{-4}$), leads to a suppression of the C_p inflection located at approximately 55% of the airfoil chord, which is associated with the laminar separation bubble and the consequent laminar-to-turbulent transition. Therefore, it is evident that an excessively large value of c_{art} results in a fully turbulent flow.

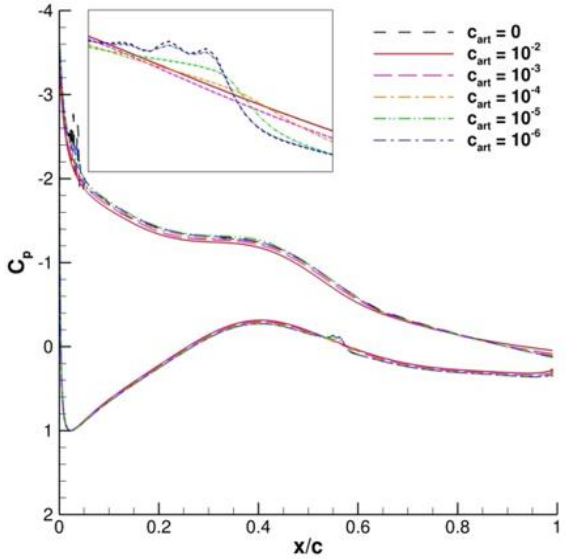


Figure 8. S809, Re = $1 \cdot 10^6$, α = 8°, effect of artificial viscosity - pressure side

Figures 9 and 10 present the aerodynamic coefficients at Re = $1 \cdot 10^6$. In line with previous findings, the stabilized versions of both the SA-R1 and SA-SMP models accurately predict the lift and drag coefficients at low to moderate angles of attack, showing good agreement with the experimental data. In the stall region, however, both approaches tend to overestimate the values of C_l and C_d. Nevertheless, the SA-R1 model is able to capture the qualitative behavior of the aerodynamic coefficients, once again demonstrating superior performance in predicting the flow field when the airfoil operates at high angles of attack.

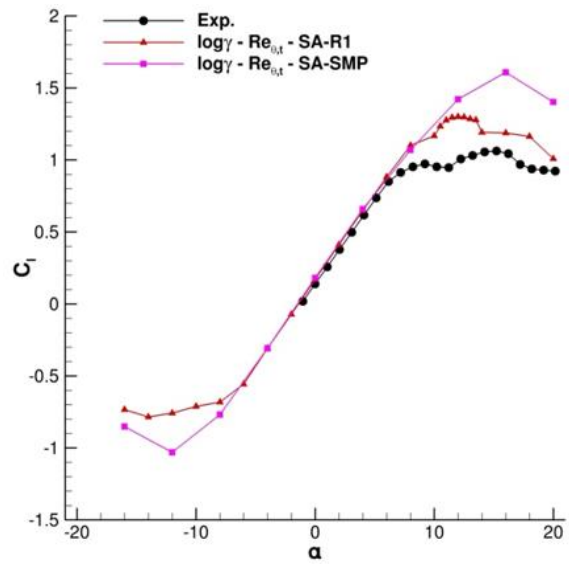


Figure 9. S809, Re = $1 \cdot 10^6$, lift coefficient

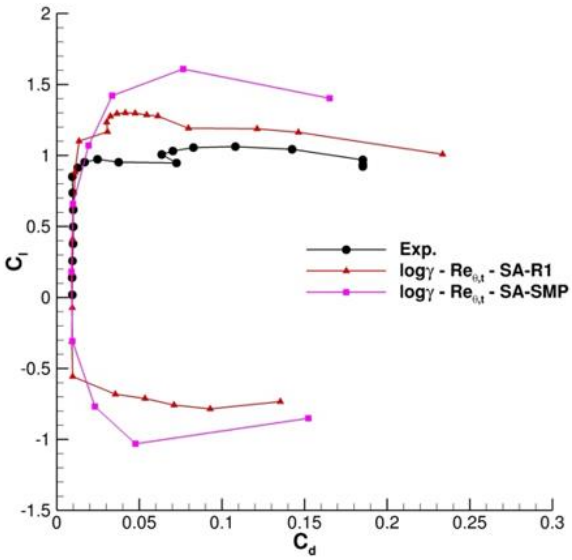


Figure 10. S809, Re = $1 \cdot 10^6$, eiffel polar

5. CONCLUSIONS

This paper has presented recent advances in the development of local correlation-based laminar-to-turbulent transition models built upon the SAs turbulence equation, with a specific focus on their application to wind turbine airfoil aerodynamics. The proposed framework incorporates three key numerical ingredients designed to improve robustness and reliability of the $\gamma - \widetilde{Re}_{\theta,t}$, transition framework: a logarithmic formulation of the intermittency transport

equation to ensure the positivity of the variable, an energy-based limiting procedure to prevent excessively high values of the logarithmic variable, and a gradient-driven artificial viscosity term to suppress the Gibbs-like pressure oscillations experienced in the transition region. These strategies were combined with two formulations of the SA production term, namely the rotation correction variant (SA-R1) and the strain-modulated production approach (SA-SMP).

The effectiveness, efficiency, and robustness of the proposed models were assessed by computing the flow fields developing around a wind turbine airfoil: the S809 over a range of Reynolds numbers representative of utility-scale blade sections ($Re = 1 \cdot 10^6$ and $Re = 2 \cdot 10^6$). The results obtained are globally satisfactory. Both the SA-R1 and SA-SMP formulations accurately reproduce the pressure coefficient distributions and the aerodynamic coefficients at low to moderate angles of attack, capturing the laminar-to-turbulent transition of the boundary.

In cases where Gibbs-like oscillations were observed near the transition region, the gradient-driven artificial viscosity proved effective in recovering a physically consistent solution without altering the predicted transition behavior. This holds true when the scaling coefficient c_{art} is chosen with care. In fact, too low values are not sufficient to damp the numerical fluctuations, while excessively large values of c_{art} were found to suppress the laminar separation bubble, leading to a fully turbulent flow field.

In the stall region, the models exhibit the overestimation of aerodynamic force coefficients that is commonly observed with RANS-based approaches, and the present results are consistent with this well-known limitation. Nevertheless, within this region the SA-R1 model consistently shows slightly superior performance compared to SA-SMP: it provides closer agreement with the experimental lift curve near and beyond stall, and yields drag coefficient predictions that are more consistent with the reference experimental data.

REFERENCES

[1] Menter, F., Langtry, R., Likki, S., Suzen, Y., Huang, P., Volker, S. (2006) A correlation-based transition model using local variables - Part 1: Model formulation. Journal of Turbomachinery, 128(3): 413-422. https://doi.org/10.1115/1.2184352

[2] Menter, F., Langtry, R., Volker, S. (2006). Transition modelling for general purpose CFD codes. Flow, Turbulence and Combustion, 77(1): 277-303. https://doi.org/10.1007/s10494-006-9047-1

[3] Spalart, P., Allmaras, S. (1992). A one-equation turbulence model for aerodynamic flows. AIAA Paper No. 92-0439.

[4] Medida, S., Baeder, J.D. (2011). Application of the correlation-based γ-Reθ,t transition model to the Spalart-Allmaras turbulence model. AIAA Paper No. 2011-3979.

[5] D'Alessandro, V., Montelpare, S., Ricci, R., Zoppi, A., (2017). Numerical modeling of the flow over wind turbine airfoils by means of Spalart-Allmaras local correlation based transition model. Energy, 130: 402-419. https://doi.org/10.1016/j.energy.2017.04.134

[6] D'Alessandro, V., Montelpare, S., Ricci, R. (2021). Assessment of a Spalart-Allmaras model coupled with local correlation based transition approaches for wind turbine airfoils. Applied Sciences, 11(4): 1872. https://doi.org/10.3390/app11041872

[7] D'Alessandro, V., Falone, M., Giammichele, L., Ricci, R., (2025). A robust intermittency equation formulation for transition modeling in Spalart-Allmaras simulations of airfoil flows over a wide range of Reynolds numbers. Physics of Fluids, 37(11): 114121. https://doi.org/10.1063/5.0294697

[8] Dacles-Mariani, J., Zilliac, G., Chow, J., Bradshaw, P. (1995). Numerical/experimental study of a wingtip vortex in the near field. AIAA Journal, 33(9): 1561-1568. https://doi.org/10.2514/3.12826

[9] Baldwin, B., Barth, T. (1990). A one-equation turbulence transport model for high Reynolds number wall-bounded flows. NASA - Report No. TM-102847

[10] Allmaras, S.R., Johnson, F.T. (2012). Modifications and clarifications for the implementation of the Spalart-Allmaras turbulence model. In Seventh International Conference on Computational Fluid Dynamics (ICCFD7), Big Island, Hawaii, pp. 1-11.

[11] DM, S. (1997). Design and experimental results for the S809 airfoil. Technical Report NREL/SR-440-6918, DE97000206, National Renewable Energy Laboratory (NREL), Golden, CO.